Direct simulations of spherical particle motion in Bingham liquids

Prashant, J.J. Derksen*

Chemical & Materials Engineering Department, University of Alberta, ECERF 7-028, Edmonton, Alberta T6G 2G6, Canada

ARTICLE INFO

ABSTRACT

The present work deals with the development of a direct simulation strategy for solving the motion of spherical particles in a Bingham liquid. The simulating strategy is based on a lattice-Boltzmann flow solver and the dual-viscosity Bingham model. Validation of the strategy is first performed for single phase (lid-driven cavity flow) and then for two phase flows. Lid-driven cavity flow results illustrate the flow's response to an increase of the yield stress. We show how the settling velocity of a single sphere sedimenting in a Bingham liquid is influenced by the yield stress of the liquid. The hydrodynamic interactions between two spheres are studied at low and moderate Reynolds number. At low Reynolds number, two spheres settle with equal velocity. At moderate Reynolds number, the yield effects are softened and the trailing sphere approaches the leading sphere until collision occurs.

1. Introduction

Bingham liquids, a special subclass of viscoplastic liquids, possess a yield stress which must be exceeded before the liquid shows any significant deformation. By virtue of its yield stress, a Bingham liquid is capable of trapping an embedded particle for a long time. For example, drilling liquids used in petroleum industry posses a yield stress and prevent the settling of rock debris when their circulation is stopped (Peysson, 2004). The presence of a yield stress in various industrial liquids is critical to solid–liquid suspensions. In oil sand operations (Masliyah, Zhou, Xu, Czarnecki, & Hamza, 2004), clay particles get surface activated in the presence of water and make a complex clay–water suspension. This complex suspension possesses a yield stress which is relevant for the design, operation and efficiency of oil sands processing, especially in those parts of the process related to separation and to tailings. If the net gravity force acting on inert particles (sand, bitumen drops) is not enough to overcome the yield stress, they are trapped in the clay network hindering gravity based separation.

Research studies focused on spheres sedimenting in Bingham liquids date back several decades. Ansley and Smith (1967) postulated the shape and extent of yielded/unyielded regions surrounding the sphere using slip line theory. In a classical work, Beris, Tsamopoulos, Armstrong, and Brown (1985) numerically determined the velocity field, pressure field, shape of the yield surfaces and drag coefficient for the creeping flow around a sphere in an unbounded Bingham liquid. Blackery and Mitsoulis (1997) reported

drag coefficients for bounded flows with various tube/sphere diameter ratios. More recently Liu, Muller, and Denn (2002) and Yu and Wachs (2007) obtained the shape and extent of yielded/unyielded regions for such flow systems. Turning the attention towards sedimentation of more than one sphere, one finds few results for Bingham liquids, probably due to the complexity associated with two sphere motion in addition to the discontinuous nature of Bingham liquid model. Liu, Muller, and Denn (2003) numerically investigated the creeping flow of two identical spheres falling collinearly along the axis of a circular cylinder in a Bingham liquid. They calculated the yield surfaces as a function of the ratio of the center to center distance over the radius of the spheres and further predicted a plug like (unyielded) region between the two spheres along the symmetry axis. In an experimental work, Merkak, Jossic, and Magnin (2006) reported an appreciable hydrodynamic interaction between two spheres falling one above the other. They proposed drag coefficient correlations and showed that the yield effect of viscoplastic liquids reduces the degree of interaction compared to sedimentation in Newtonian liquid. Yu and Wachs (2007) examined the motion of two spheres translating along the axis of a tube at low Reynolds number and predicted a higher velocity of two spheres than a single sphere due to the hydrodynamic interaction.

One of the difficulties encountered in implementing the Bingham model in a computer code is its non-differentiable form. There are mainly three approaches which have been used in the literature to counter these problems: the dual-viscosity model (Beverly & Tanner, 1992; O'Donovan & Tanner, 1984), regularization methods (Mitsoulis & Zisis, 2001; Papanastasiou, 1987), and variational inequality based methods (Vola, Boscardin, & Latche, 2003; Yu & Wachs, 2007). The first two methods approximate the Bingham model by considering the solid region as a highly viscous mate-

---

* Corresponding author. Tel.: +1 780 492 5267; fax: +1 780 492 2881.
E-mail address: jos@ualberta.ca (J.J. Derksen).

rial. The variational inequality method is rigorously equivalent to the original Bingham model, and is implemented by introducing Lagrange multipliers.

The present work concentrates on the sedimentation of particles in Bingham liquid using the lattice-Boltzmann method (LBM) as flow solver. First we discuss and analyse the results of single sphere sedimentation at low Reynolds number. We then investigate the hydrodynamic interaction between the two spheres falling along the axis of symmetry at low and moderate Reynolds number. Hydrodynamic interaction is interpreted in terms of settling velocity, flow field and attraction between the spheres. The (benchmark) results presented in this paper are meant to assess the accuracy and potential of the computational method so that (in future work) the method can be used for flow systems relevant to industrial and environmental processes, such as the simulation of dense solid–liquid suspensions involving Bingham liquids.

This paper is organized as follows: in Section 2 a brief introduction to LBM, the Bingham model and dimensionless numbers is provided. Validation of the numerical procedure is accomplished by comparing results for lid-driven cavity flow with results from the literature (Section 3). In Section 4 we study the single sphere sedimentation in Bingham liquid in a confined domain and report the effects of yield stress on the settling velocity. In Section 5, we examine the sedimentation of two spheres (one above the other) in Bingham liquid at low and moderate Reynolds number. The concluding remarks are provided in Section 6.

2. Numerical model

2.1. Flow solver

The lattice-Boltzmann method is a well established and frequently used method for simulating liquid flows. In principle it has a second order accuracy in space and time and is particularly regarded an efficient flow solver for flows involving interfacial dynamics and complex geometries (Chen & Doolen, 1998). LBM originated from lattice gas automata in which liquid particles are distributed on a lattice of nodes. Each liquid particle has certain directions of velocities at each node. At each time step a liquid particle is involved in two sequential processes: streaming and collision. In the streaming process, the liquid particle moves from one node to the nearest node in the direction of its velocity and in collision it interacts with other liquid particles reaching the same node and changes its velocity as per collision rules. In this work, we make use of the formulation by Eggels and Somers (1995) which is a D3Q18 model (three-dimensional, 18 velocities). In LBM the units of distance and time are the lattice spacing and the time step, respectively. All the liquid properties and flow variables are scaled to dimensionless quantities within certain ranges (e.g. for density and kinematic viscosity: $\rho \sim 8$, $0.25 > \nu > 10^{-5}$) (Eggels & Somers, 1995). The bounce-back scheme is a popular way to mimic no-slip boundary conditions at plane walls. In this scheme, the liquid particle is reflected back to the node it comes from. Explicitly applying zero velocity on boundaries is an alternative to retrieve the no-slip condition. No-slip boundary condition at a curved boundary is achieved by a forcing method (Derksen & Van den Akker, 1999), also known as immersed boundary method.

2.2. Bingham model

Viscoplastic liquids possess a yield stress (τ_0) which must be exceeded before the fluid shows any significant deformation. The Bingham model, one of the simplest rheological models, is used to describe the flow properties of liquid with a yield stress τ_0. The deformation rate remains zero and the material behaves like a solid
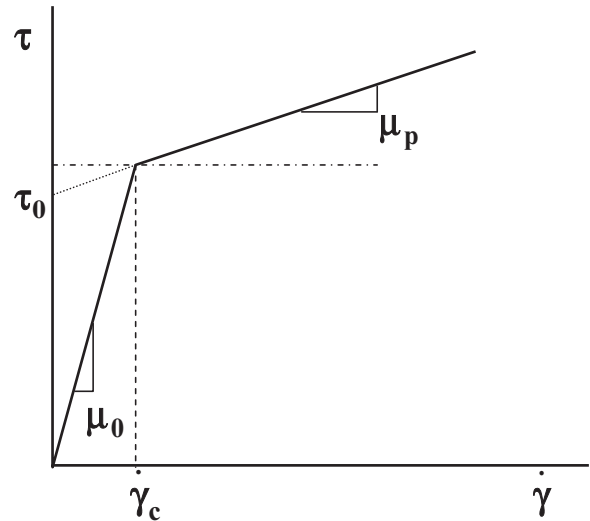

Fig. 1. One-dimensional representation of dual-viscosity Bingham model.

until the stress exceeds the yield limit of the liquid. In a generalized manner, the constitutive equations for a Bingham liquid can be written as

$$\tau_{ij} = 2 \left(\frac{\tau_0}{\dot{\gamma}} + \mu_p \right) d_{ij} \quad |\tau| > \tau_0 \tag{1}$$

$$d_{ij} = 0 \quad |\tau| < \tau_0 \tag{2}$$

In the above expressions, τ_{ij} is deviatoric part of whole stress tensor σ_{ij}, $\dot{\gamma}$ is the deformation rate ($\dot{\gamma} = \sqrt{d_{ij}d_{ij}}$), d_{ij} is the rate of deformation tensor [$1/2((\partial u_i/\partial x_j)+(\partial u_j/\partial x_i))$], μ_p is the plastic viscosity, and $|\tau|$ is the magnitude of the shear stress ($|\tau| = \sqrt{\tau_{ij}\tau_{ij}}$).

In the present work, a dual-viscosity model is used to mimic Bingham liquids (Beverly & Tanner, 1992) because of its less complex structure and easy implementation within the lattice-Boltzmann scheme, which essentially is a viscous flow solver. In this model the region around zero shear rate is characterized by a highly viscous material with viscosity μ_0. At higher shear the actual Bingham rheology is represented by a much lower plastic viscosity μ_p. The one-dimensional dual-viscosity Bingham rheology is shown in Fig. 1. The transition (from high to low viscosity) gives rise to a critical shear rate $\dot{\gamma}_c = \tau_0/(\mu_0 - \mu_p)$. When the shear rate ($\dot{\gamma}$) becomes greater than critical shear rate, material is considered yielded. Thus the criterion of yielded and unyielded regions is defined as

$$\dot{\gamma} > \dot{\gamma}_c \rightarrow \text{yielded} \tag{3}$$

$$\dot{\gamma} \leq \dot{\gamma}_c \rightarrow \text{unyielded} \tag{4}$$

In the dual-viscosity model, the apparent viscosity (μ_a) and shear stress (τ_{ij}) of the material are written as

$$\mu_a = \mu_0 \quad \dot{\gamma} \leq \dot{\gamma}_c \tag{5}$$

$$\mu_a = \mu_p + \frac{\tau_0}{\dot{\gamma}} \quad \dot{\gamma} > \dot{\gamma}_c \tag{6}$$

$$\tau_{ij} = 2\mu_a d_{ij} \tag{7}$$

2.3. Dimensionless numbers

As the two dimensionless numbers that govern the Bingham liquid flow system we chose a Reynolds number and a Bingham number:

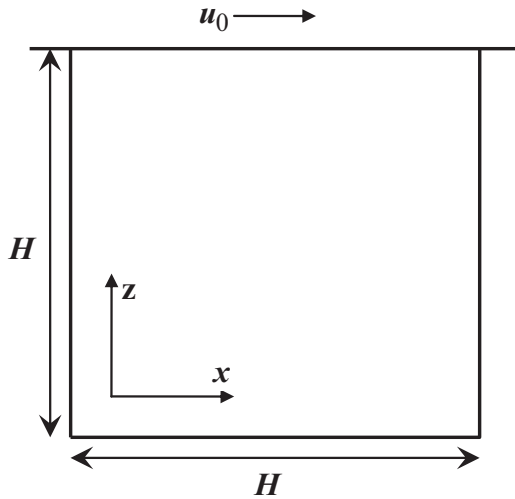$$\text{Reynolds number } Re = \frac{\rho_f U_c L_c}{\mu_p} \tag{8}$$

Fig. 2. Definition of the LDC geometry and coordinate system, its origin being in the south-west corner.

Bingham number $Bn = \dfrac{\tau_0 L_c}{\mu_p U_c}$ (9)

In the above expressions ρ_f is the density of Bingham liquid while U_c and L_c are the characteristic velocity and length, respectively. Since spherical particles are considered, we take the sphere diameter d as characteristic length. The definition of the characteristic velocity depends upon the inertial effects. We define one more (numerical) dimensionless number: the viscosity ratio μ_r. This is the ratio of zero shear viscosity to plastic viscosity, i.e. $\mu_r = \mu_0/\mu_p$.

In case of low inertial effects, the Stokes terminal velocity (U_s) for a single sphere settling in an unbounded medium with uniform viscosity μ_p is taken as characteristic velocity. U_s is defined by the notion:

$$U_c = U_s = \frac{d^2(\rho_s - \rho_f)g}{18\mu_p} \qquad (10)$$

where ρ_s is the density of solid sphere and g is the acceleration due to gravity.

In case of moderate inertial effects, the terminal velocity (U_∞) of a single sphere settling in an unbounded medium with uniform viscosity μ_p is taken as characteristic velocity. To calculate U_∞ we consider the drag coefficient expression proposed by Abraham (1970) and later used by ten Cate, Nieuwstad, Derksen, and Van den Akker (2002):

$$C_d = \frac{24}{Re}\left(1 + \frac{\sqrt{Re}}{9.06}\right)^2 \qquad (11)$$

Based on the drag coefficient defined by Eq. (11), U_∞ is given by

$$U_\infty = \frac{d^2(\rho_s - \rho_f)g}{18\mu_p(1 + \sqrt{Re}/9.06)^2} \qquad (12)$$

3. Lid-driven cavity flow

In computational fluid dynamics, lid-driven cavity flow is a widely used test case for benchmarking incompressible iso-thermal liquid flows. The flow definition and coordinate system for lid-driven cavity flow are given in Fig. 2. A Bingham liquid, contained inside a square cavity is set into motion by the upper wall which slides at constant speed. The velocity of the upper wall and the cavity depth are taken as characteristic velocity and length, respectively. Originally a three-dimensional grid is used for simulating the flow, applying no-slip boundary conditions (using the halfway
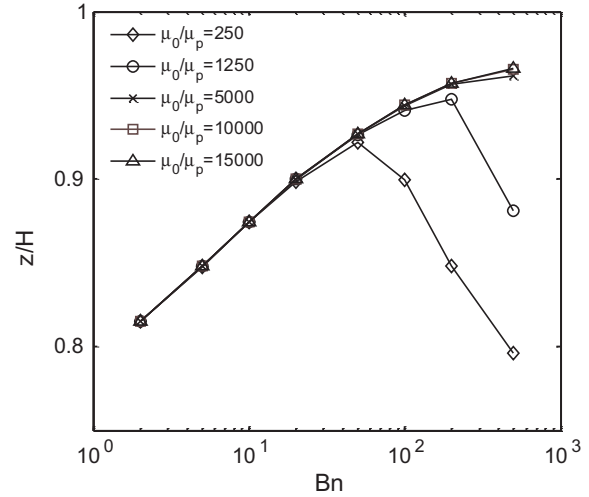

Fig. 3. Sensitivity of z-coordinate of the primary vortex center with viscosity ratio (μ_0/μ_p); grid size: $81 \times 1 \times 81$.

bounce-back scheme) at the east, west, north and south wall, where the north wall is moving. Periodic boundary conditions are imposed at front and back boundaries effectively making it a two-dimensional problem.

3.1. Verification of the numerical method

To establish the qualitative credibility of results obtained by a numerical method, it is desirable to verify the method with different numerical parameters. In this study, two parameters are investigated for the purpose of verification. One is the grid size and the other is the viscosity ratio (μ_r). Previous researches (Mitsoulis & Zisis, 2001; Vola et al., 2003; Yu & Wachs, 2007) have shown that the location of the primary vortex formed in lid-driven cavity flow is appreciably influenced by the yield stress of the Bingham liquid at low Reynolds number (the primary vortex moves closer to the moving lid as Bn increases). This change in location is an easily observable quantity. Therefore we monitor the vertical position of the primary vortex center to observe the qualitative credibility of our results. The center of the primary vortex is the point having the minimum value of the stream function (ψ) which is calculated through integration of the velocity field ($u_x = \partial \psi/\partial z$, $u_z = -\partial \psi/\partial x$).
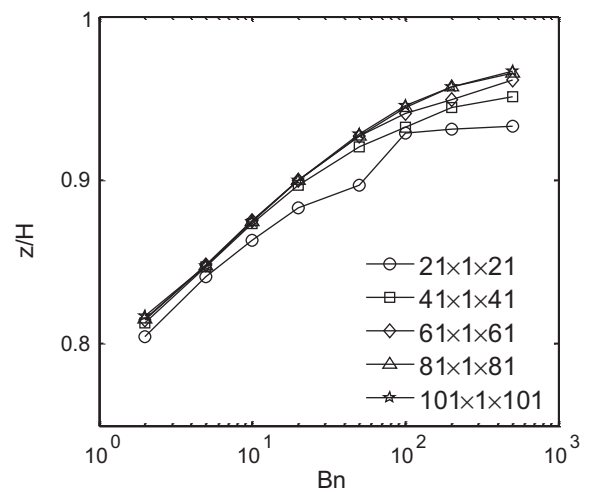

Fig. 4. Sensitivity of z-coordinate of the primary vortex center with grid size ($x \times y \times z$); $\mu_0/\mu_p = 10{,}000$.
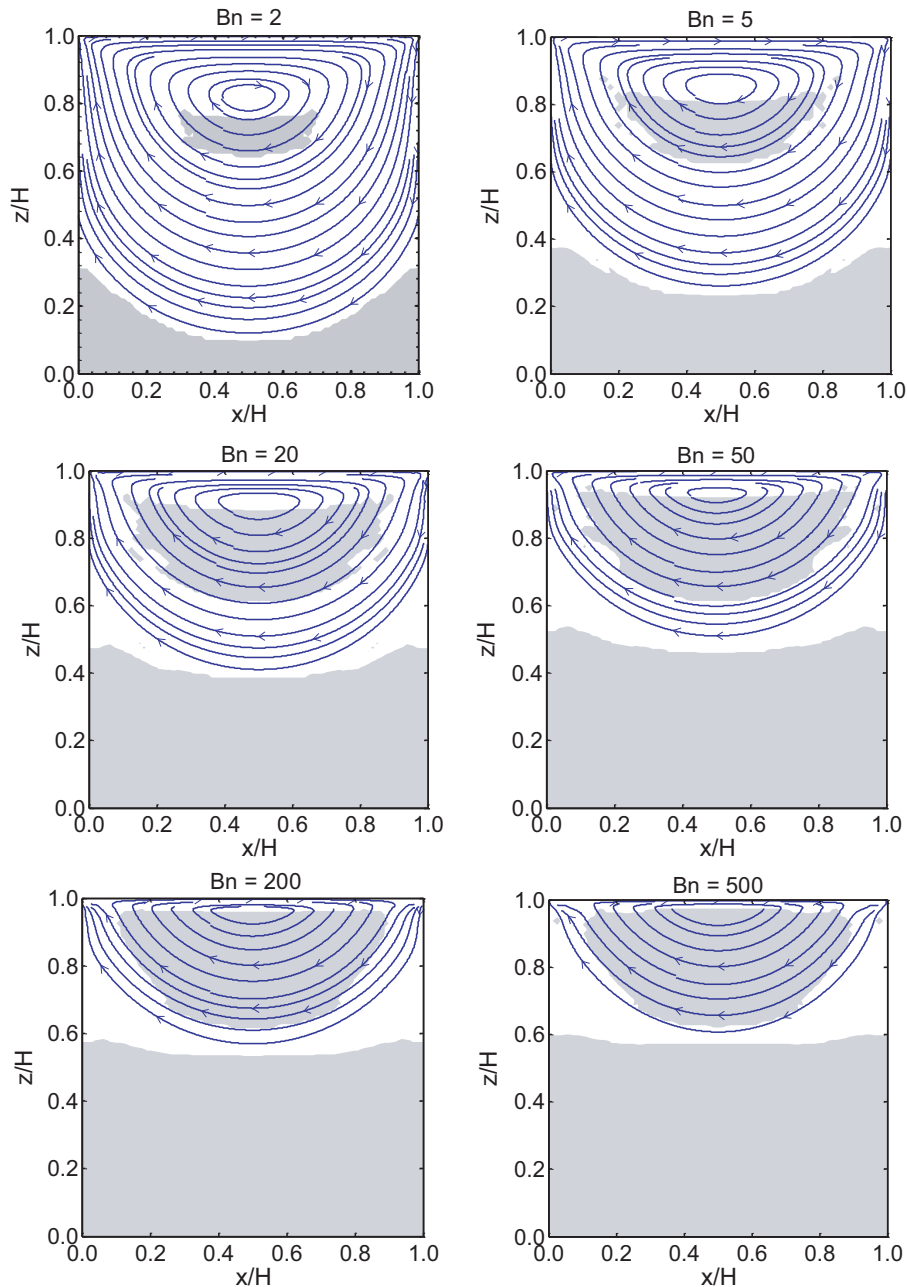
Fig. 5. Yielded (white)/unyielded (shaded) regions together with streamlines for lid-driven cavity flow of a Bingham liquid with different Bingham numbers; Re = 0.5.

In a number of previous finite element studies with the dual-viscosity Bingham model, researchers (Gartling & Phan-Thien, 1984; O'Donovan & Tanner, 1984) have found their results insensitive to the viscosity ratio if $\mu_r > 1000$. Beverly and Tanner (1992) reported the highest accuracy for an axi-symmetric problem when $\mu_r = 1000$. For the present work, different values of the viscosity ratio ($\mu_r = 250, 1250, 5000, 10,000, 15,000$) are chosen to measure the sensitivity in terms of the vertical position of the primary vortex center. For each value of μ_r, simulations (at Re = 0.5) are performed over a range of liquid's yield stress (Bn = 2, 5, 10, 20, 50, 100, 200, 500). The primary vortex position as a function of the Bingham number (Bn) for each viscosity ratio is shown in Fig. 3. For the range of investigation ($2 \leq Bn \leq 500$), the primary vortex center moves closer to the moving lid on increasing Bn only if $\mu_r > 1250$. Simulations with lower μ_r (≤ 1250) fail to deliver the expected results. This discrepancy can be attributed to the misleading veloc-

ity fields which can be generated with the dual-viscosity model, if shear stresses or shear rates developed are very low compared to yield stress (τ_0) or critical shear rate ($\dot{\gamma}_c$), respectively. By decreasing the viscosity ratio, we increase the magnitude of the critical shear rate $\dot{\gamma}_c$. If the yield stress of the liquid is high (Bn > 50), developed shear rates are very low and may fall below the critical shear rate for the lower viscosity ratios which in turn leads to unrealistic predictions of the dual-viscosity model. Fig. 3 shows that after reaching a certain value, increase of the viscosity ratio does not alter the position of primary vortex anymore. We obtain similar results with $\mu_r = 10,000$ and 15,000. Therefore we choose the value 10,000 as the default viscosity ratio.

Choosing an appropriate grid to mimic the lid-driven cavity problem is important in terms of accuracy and computational effort. Keeping all other numerical parameters unchanged, simulations are performed with five different grids and the results
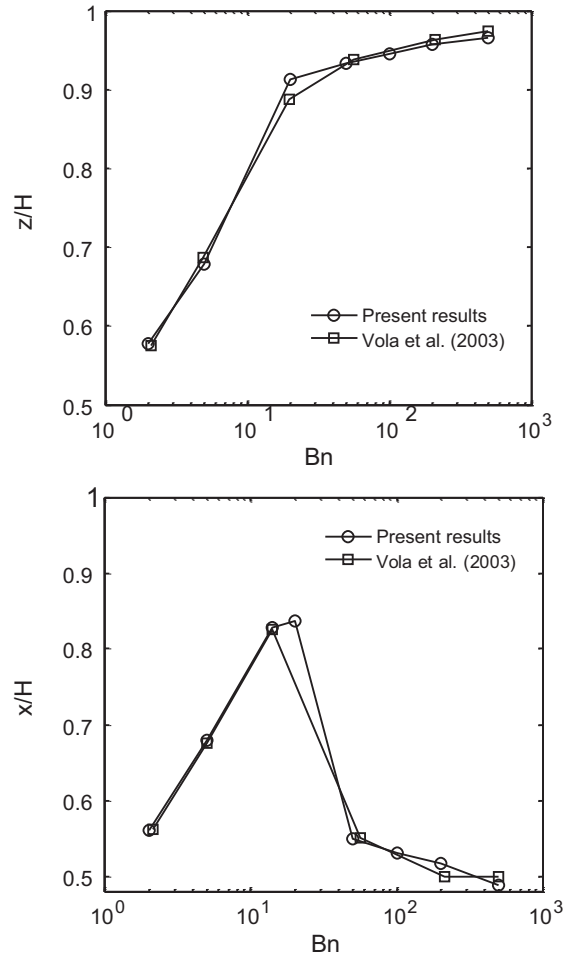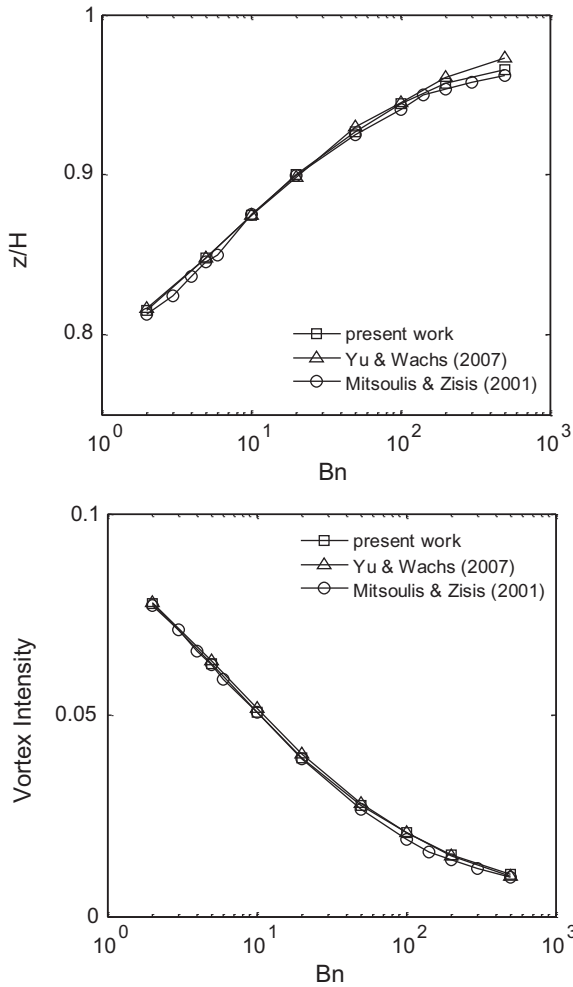
Fig. 6. Top: *z*-location of the vortex center as a function of Bn, bottom: vortex intensity at vortex center as a function of Bn; Re = 0.5; comparison with the literature results (Mitsoulis & Zisis, 2001; Yu & Wachs, 2007).

are shown in Fig. 4. Approximately identical results are observed for all grids with low Bingham numbers (Bn ≤ 50) except for the 21 × 1 × 21 grid. Results start to differ with higher Bingham numbers. For the whole range of investigation (2 ≤ Bn ≤ 500), the results obtained from grid size 81 × 1 × 81 differ little from those obtained from grid size 101 × 1 × 101. Since a finer grid (101 × 1 × 101) does not offer any significant contribution, we adhere to the grid size of 81 × 1 × 81.

3.2. Validation of the numerical method

Based on the verification of the numerical method (Section 3.1), viscosity ratio and grid size are chosen as 10,000 and 81 × 1 × 81, respectively for mimicking the lid-driven cavity flow with Bingham liquid. Simulations have been performed with various values of the Bingham number (2 ≤ Bn ≤ 500) keeping the Reynolds number constant at Re = 0.5. Streamlines coupled with yielded (white) and unyielded (shaded) regions inside the cavity with Bn = 2, 5, 20, 50, 200 and 500 are displayed in Fig. 5. In unyielded regions the deformation rate is below the critical shear rate $\dot{\gamma}_c$. The unyielded regions in the cavity can be divided in two categories: (a) a lower unyielded region (close to the bottom wall) (b) an upper unyielded region (close to the moving lid). Since the lid (top wall) is the only source to generate shear stress, the effect imparted to the lower region is not sufficient to yield the liquid. The formation of the upper unyielded region takes place due to the existence
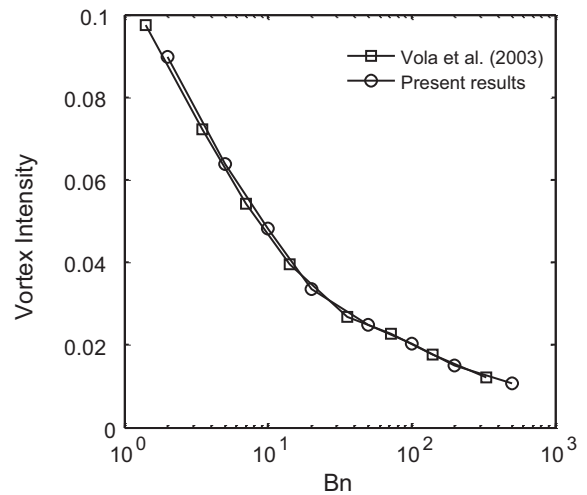

Fig. 7. *z*-location (top) and *x*-location (center) of the vortex center as a function of Bn; bottom: vortex intensity at vortex center as a function of Bn; Re = 1000; comparison with the literature result (Vola et al., 2003).

of the primary vortex in which the deformation rate is very small. Both unyielded regions grow with the increase of the Bingham number. It is interesting to observe the streamlines inside a cavity (refer Fig. 5). Ideally, unyielded regions are solid regions and they should be quiescent. In the present study the streamlines pass through unyielded regions because these regions are not truly solid (they are highly viscous with viscosity μ_0). This also could explain the deviations in terms of the shape of the
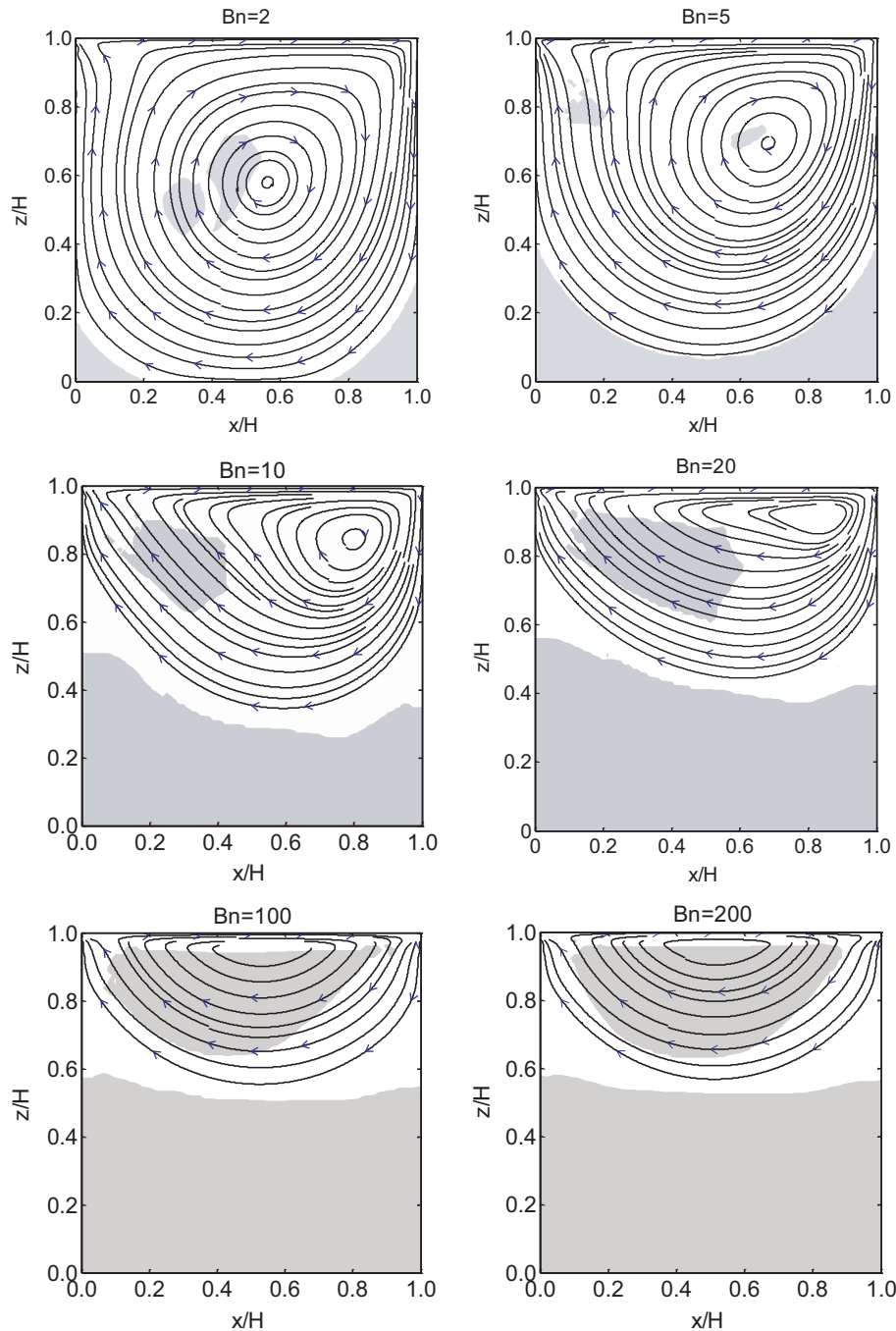
Fig. 8. Yielded (white)/unyielded (shaded) regions together with streamlines for lid-driven cavity flow of a Bingham liquid with different Bingham numbers; Re = 1000.

unyielded regions as compared to shapes reported by Yu and Wachs (2007).

Other quantities of interest are the position of the primary vortex and the vortex intensity at its center. Vortex intensity is defined as $-\psi^*_{min}$ at the center of the vortex where ψ^* denotes the dimensionless stream function. In the present work the dimensionless stream function is evaluated from the notion $\psi^* = \psi/u_0 H$. A comparison of quantities obtained from this study with the literature is shown in Fig. 6. The position of the primary vortex is a distinct function of the Bingham number. As the yield stress (τ_0) of the liquid increases, it restricts the flow zone to close to the moving lid, making regions away from the lid less active. The physical concept of stream function (ψ) is associated with the volumetric flow rate of liquid. With the increase of the Bingham number, the liquid's

resistance to lid motion becomes higher which decreases the volumetric flow rate at the primary vortex center. Therefore the vortex intensity decreases with the increase of the yield stress of the liquid.

3.3. Effect of the Reynolds number

We now move to higher Reynolds numbers. First we validate our numerical method with the results available in the literature at Re = 1000 (Vola et al., 2003). The grid size is the same as in the low Reynolds number study, i.e. $81 \times 1 \times 81$. Given the results to come, this proves to be a good resolution. The simulations cover a range of Bingham numbers ($2 \leq Bn \leq 500$) at Re = 1000. The comparison of results with the literature is presented in Fig. 7. Then in Fig. 8 the plots of the streamlines and the rigid zones with
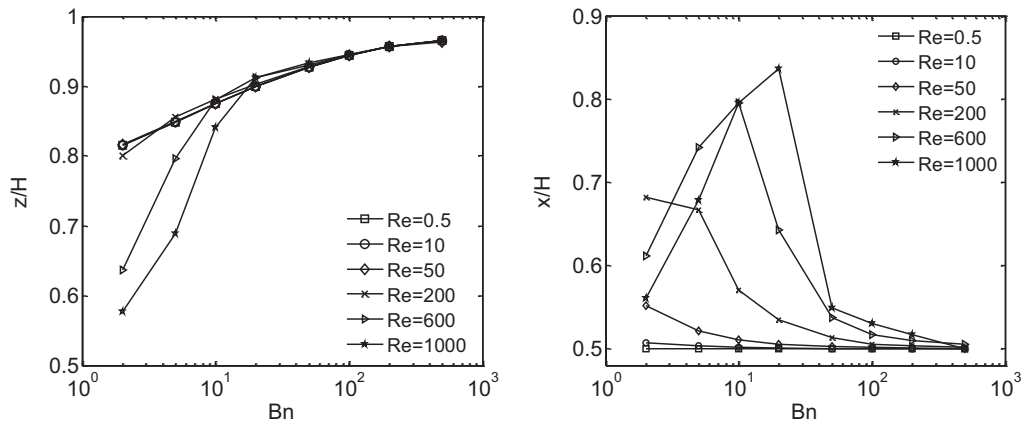
Fig. 9. *z*-location (left) and *x*-location (right) of the vortex center as a function of Bn; Re = 0.5, 10, 50, 200, 600 and 1000.

various Bingham numbers are shown. It is observed that vortex intensities obtained from our simulations agree well with those reported by Vola et al. (2003). While comparing the results for the vertical position of the primary vortex center, we see a deviation of around 3% and 1% with Vola et al. (2003) at Bn = 20 and Bn = 500, respectively. Comparison of the horizontal position data is also in close agreement within the range of ($2 \leq$ Bn ≤ 100). At small Bingham numbers (Bn ≤ 20) the primary vortex shifts horizontally towards the east wall of the cavity. As the yield stress is increased further, the viscous effects dominate and the primary vortex moves back to the middle of the cavity. The primary vortex center attains the maximum horizontal position ($x/H = 0.837$) if Bn = 20.

Fig. 9 shows the positions (horizontal and vertical) of the primary vortex center with different Bingham numbers, at Re = 0.5, 10, 50, 200, 600 and 1000. The vertical position of the primary vortex does not change significantly till Re = 50 (0.1% change from Re = 0.5 with Bn = 2). An appreciable change in vertical position is observed with low Bingham numbers at Re = 600 and 1000. When inertial effects are highly dominating, a Bingham liquid behaves like a Newtonian liquid. At Re = 1000, the value of the vertical position of the primary vortex center at Bn = 2 ($z/H = 0.577$) obtained by this study

is close to the value ($z/H = 0.565$) of the same quantity observed by Botella and Peyret (1998) with Newtonian liquid. As the yield stress of the liquid increases, the inertial effects are softened and regions away from the moving lid get less active, drawing the vortex closer to the lid and we obtain results similar to those at low Reynolds number. The horizontal position of the primary vortex center is significantly affected with low yield stress liquids beyond Re = 10. A definite trend is observed in the variation of horizontal position with Bingham number until Re is 50. With Re = 600 and 1000, a huge deviation is observed from the trend. Within a certain range of Bingham number (Bn ≤ 20 for Re = 1000 and Bn ≤ 10 for Re = 600) the vortex center travels towards the east wall irrespective of the increase of yield stress. As yield stress further increases, inertial effects are softened and the horizontal position follows the trend observed at low Re. It is interesting to note here that the horizontal position of the primary vortex center is more sensitive (as compared to vertical position) to the Reynolds number. Moreover, there seems to be a critical Bingham number at a particular Reynolds number where the flow abruptly changes its behavior. In the present study, this critical Bingham number lies in the range of $20 \leq$ Bn ≤ 50 if Re = 1000. If Re = 600 the critical Bingham number lies in the range of $10 \leq$ Bn ≤ 20.
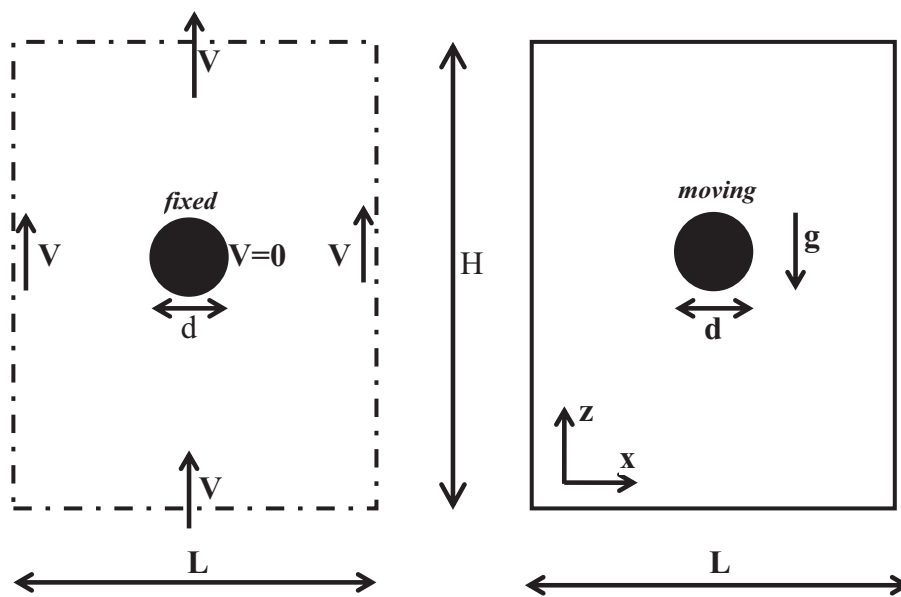

Fig. 10. Flow definition of a single sphere motion in a cylinder of square cross-section ($L \times L$) filled with Bingham liquid; (left) The liquid and cylinder walls move with velocity *V* while sphere is fixed; (right) The sphere falls under the influence of gravity, the liquid and cylinder walls are stationary.

4. Single sphere sedimentation

The interaction of a single sphere with Bingham liquid inside a cylinder has been dealt with in two ways. In the first way the sphere is assumed stationary while the liquid and the cylinder walls move with a constant velocity (flow past fixed sphere). This scheme is easier to implement since it eliminates the time dependence associated with a sphere moving relative to the computational grid. In the other scheme, the liquid and cylinder walls are stationary while the sphere falls in the cylinder under the influence of an external body force. We study both cases here. Their flow definitions are shown in Fig. 10. In the case of the fixed sphere problem, the imposed velocity V is taken as the characteristic velocity and dimensionless numbers are suffixed with the letter T (e.g. Re_T, Bn_T). While handling the problem of a moving sphere, the characteristic velocity is Stokes settling velocity U_s (considering $\mu = \mu_p$) and dimensionless numbers are suffixed with the letter S (e.g. Re_S, Bn_S).

In our simulations the spheres fall in cylinders with square cross-sections whereas most literature results deal with round cross-sections. For Newtonian fluids at low Reynolds number conditions differences between the two situations have been quantified by Miyamura, Iwasaki, and Ishii (1981). They report typically 5% differences in terms of settling velocities. For Bingham liquids at low Reynolds numbers we expect smaller differences given the presence of unyielded regions away from the sphere and close to the cylinder walls.

4.1. Fixed sphere case

Before demonstrating the results, we revisit the flow definition depicted by Fig. 10. A sphere remains fixed inside a three-dimensional square cylinder which moves along with Bingham liquid with a uniform velocity V. This velocity V is taken as the terminal velocity of the sphere in Bingham liquid. The boundary conditions are, uniform velocity V along the cylinder walls and at inlet–outlet while no-slip at the surface of sphere. Once V and other liquid parameters (ρ_f, μ_p and τ_0) are fixed, one can set the dimensionless numbers Re_T and Bn_T. In a number of previous studies (Beris et al., 1985; Blackery & Mitsoulis, 1997; Yu & Wachs, 2007) researchers have measured the ratio of Stokes velocity over terminal velocity (termed as Stokes drag coefficient by Beris et al. (1985)) as a function of the yield stress of a Bingham liquid at very low Reynolds number. In this case too, for the sake of comparison, we solve for the drag force (D) exerted on the sphere by the liquid and further calculate the Stokes velocity (U_∞) using the relation $D = 3\pi d \mu U_\infty$ (with viscosity $\mu = \mu_p$). To avoid conflict with the classical drag coefficient definition, we refrain from using the term Stokes drag coefficient and call it the velocity ratio which is defined as $v_r = U_\infty/V$. To have creeping flow, the Reynolds number chosen is very small ($Re = 0.001$) and we use a square cylinder with size $4 \times 4 \times 6$ ($L/d \times L/d \times H/d$). The spatial resolution of the simulations is such that the sphere diameter d spans 12 lattice spacings. Grid effect studies in earlier work (Derksen & Sundaresan, 2007; Derksen, 2008) showed that (at least at lower Reynolds numbers) this is sufficient resolution. The simulations are performed over a range of yield stresses such that $Bn_T = 0.1, 1, 5, 10, 20, 50, 100, 200$. The velocity ratio is calculated for each case. A depiction of the effect of the yield stress is presented in Fig. 11. The unyielded regions grow with the increase of yield stress and the interaction of the yielded Bingham liquid with the cylinder walls decreases. These results qualitatively agree with the results reported by Blackery and Mitsoulis (1997). The occurrence of polar caps (two unyielded regions at stagnation points), observed by both Beris et al. (1985) and Blackery and Mitsoulis (1997), and solid regions on either side of sphere with $Bn_T = 5, 50$ found by Ansley and Smith (1967) supports the validity of our results.
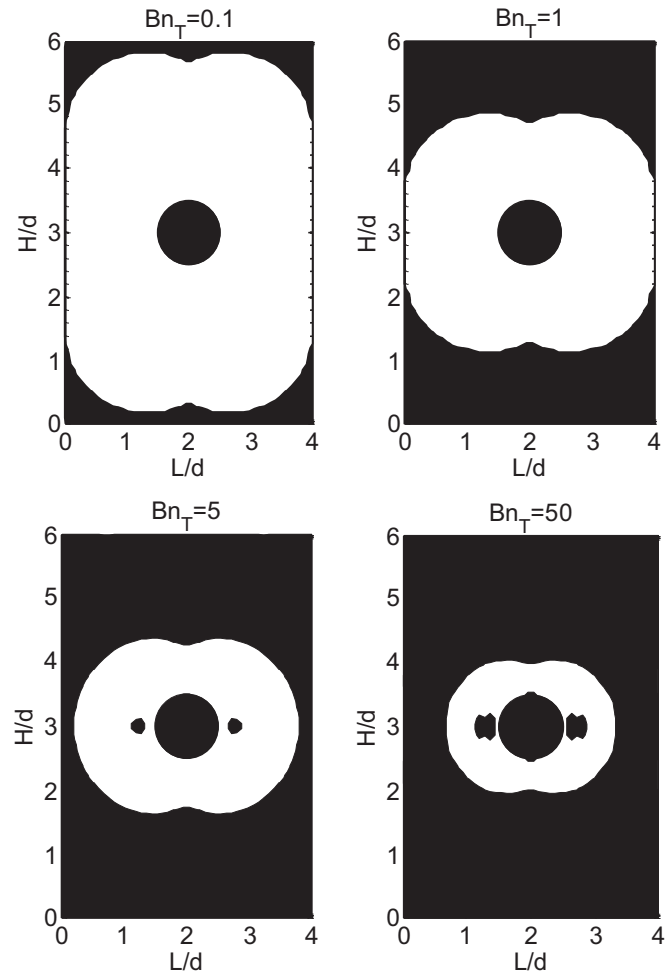

Fig. 11. The yielded (white) and unyielded (black) regions for flow of a Bingham liquid around a fixed sphere contained in a square cylinder with 4:1 ratio of L/d.

A quantitative comparison of our results with the literature is shown in Fig. 12. If we increase the yield stress of the liquid, it assists the resistance offered by the fixed sphere to the motion of the liquid. Since the liquid travels with a constant velocity V in
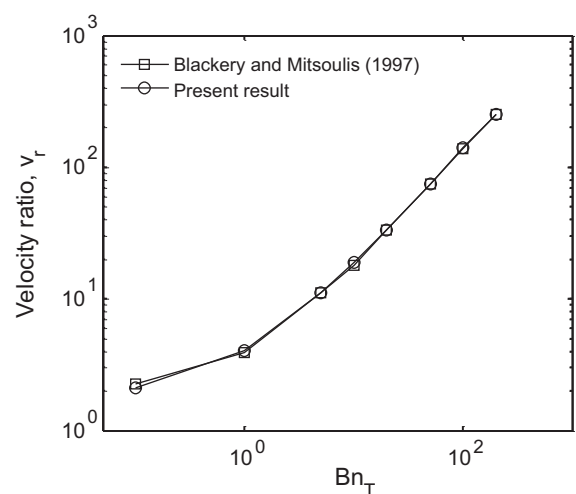

Fig. 12. Velocity ratio (v_r) as a function of Bingham number (Bn_T) when sphere remains fixed; $Re_T = 0.001$; comparison with the literature results (Blackery & Mitsoulis, 1997).

Table 1
Velocity ratio (v_r) as a function of Bingham number (Bn_T).

Bn_T	0.1	1	10	20	50	200	
v_r (Blackery and Mitsoulis)	2.24	3.92	18.04	33.13	74.11	250.25	R1
v_r (Present work)	2.10	4.06	18.84	33.47	74.77	252.96	R2
% difference $[(R2 - R1)/R2] \times 100$	−6.66	3.45	4.25	1.02	0.88	1.07	

all the simulations, the drag force exerted on the sphere increases with increase of the yield stress. This increased drag force leads to the increased Stokes velocity and thus increased velocity ratio. There is a slight difference between the flow definitions used by us. Blackery and Mitsoulis (1997) used a cylinder with circular cross-section whose diameter is four times the diameter of sphere while we have used a cylinder with square cross-section whose sides are four times the diameter of the sphere. In a square cylinder we expect the retardation effect of the walls to be less than the circular cylinder and we expect smaller velocity ratios (U_∞/V) than those obtained by Blackery and Mitsoulis (1997). One should be critical about the apparent excellent agreement of results obtained by both the studies (refer Fig. 12). It is important to note that both the axes are logarithmic which hides the minor deviation in the results. The actual deviations between the results shown in Fig. 12 are displayed in Table 1.

Miyamura et al. (1981) performed experiments to calculate the wall factors of a single solid sphere settling in a square cylinder filled with a Newtonian liquid and then compared them with the wall factors obtained with circular cylinder (Iwaoka & Ishii, 1979) keeping other parameters unchanged. They reported that the retardation effect on the terminal velocity due to wall proximity is less severe with square cylinder and the sphere settles with a greater terminal velocity which is around 5% higher than that measured with circular cylinder. Close to the Newtonian limit ($Bn_T = 0.1$), we too observe a 6.6% lesser velocity ratio (i.e. 6.6% higher terminal velocity) which is in close agreement with the results reported by

Miyamura et al. (1981). Once the yield stress of the liquid is appreciably high ($Bn_T > 0.1$), the unyielded region around the sphere grows progressively (refer Fig. 11) which restricts the interaction of the flow field with the walls. Therefore in this scenario, it is expected that the effects of the difference in cylinder geometry get smaller at higher yield stress. This is well supported by the minor deviations (shown in Table 1) observed with higher yield stress flow simulations.

4.2. Moving sphere case

We now turn our attention to the problem with a different flow definition where the sphere falls in a stationary square cylinder filled with Bingham liquid under the influence of gravitational force (refer Fig. 10). A zero velocity boundary condition is imposed along all boundaries and the no-slip boundary condition is considered for the surface of the sphere. The numerical parameters and grid size used in this case remain the same as with the fixed sphere and moving walls (Section 4.1). It is important to mention here that in this case our objective is to obtain the terminal velocity V of the sphere settling in a Bingham liquid. The gravitational force is set in such a way that Reynolds number $Re_S = 1$. The primary reason of choosing this relatively high Reynolds number is the availability of work in the literature with which we want to compare our simulations. Also, by choosing $Re_S = 1$, the effective Reynolds numbers (based on the actual terminal velocity of the sphere and μ_p) are of the order of 10^{-1} to 10^{-2} which are still fairly low Reynolds numbers.
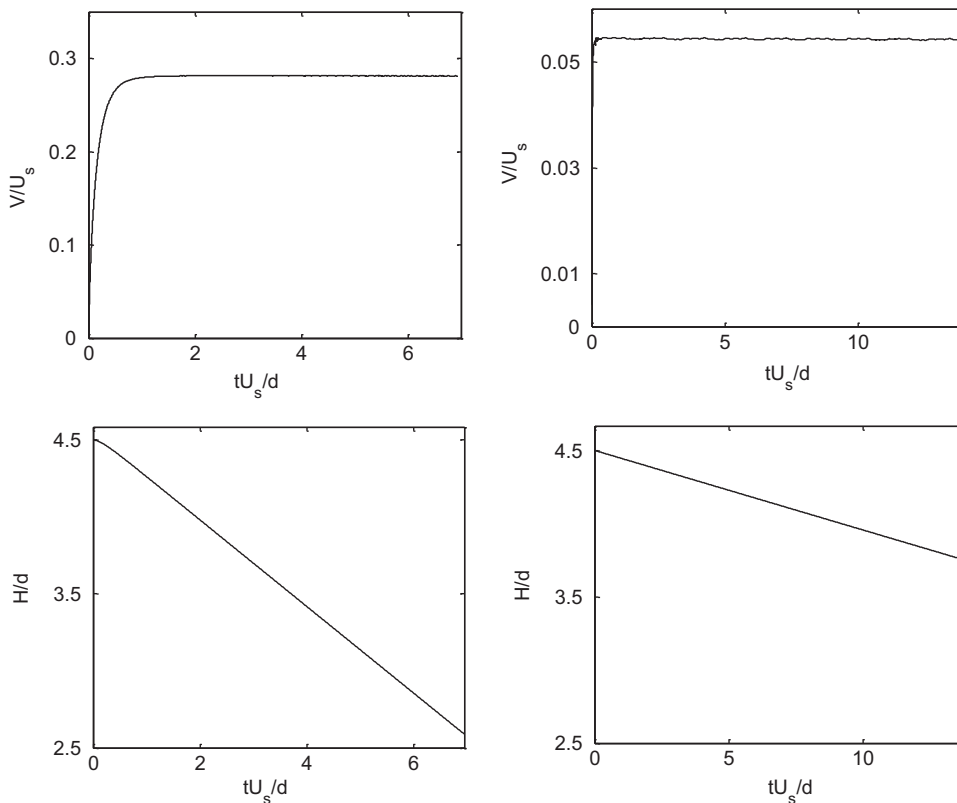

Fig. 13. Time series of settling velocity (V) and distance traveled in Bingham liquid with $Bn_S = 0.21$ (left panel) and 0.53 (right panel); $Re_S = 1$.
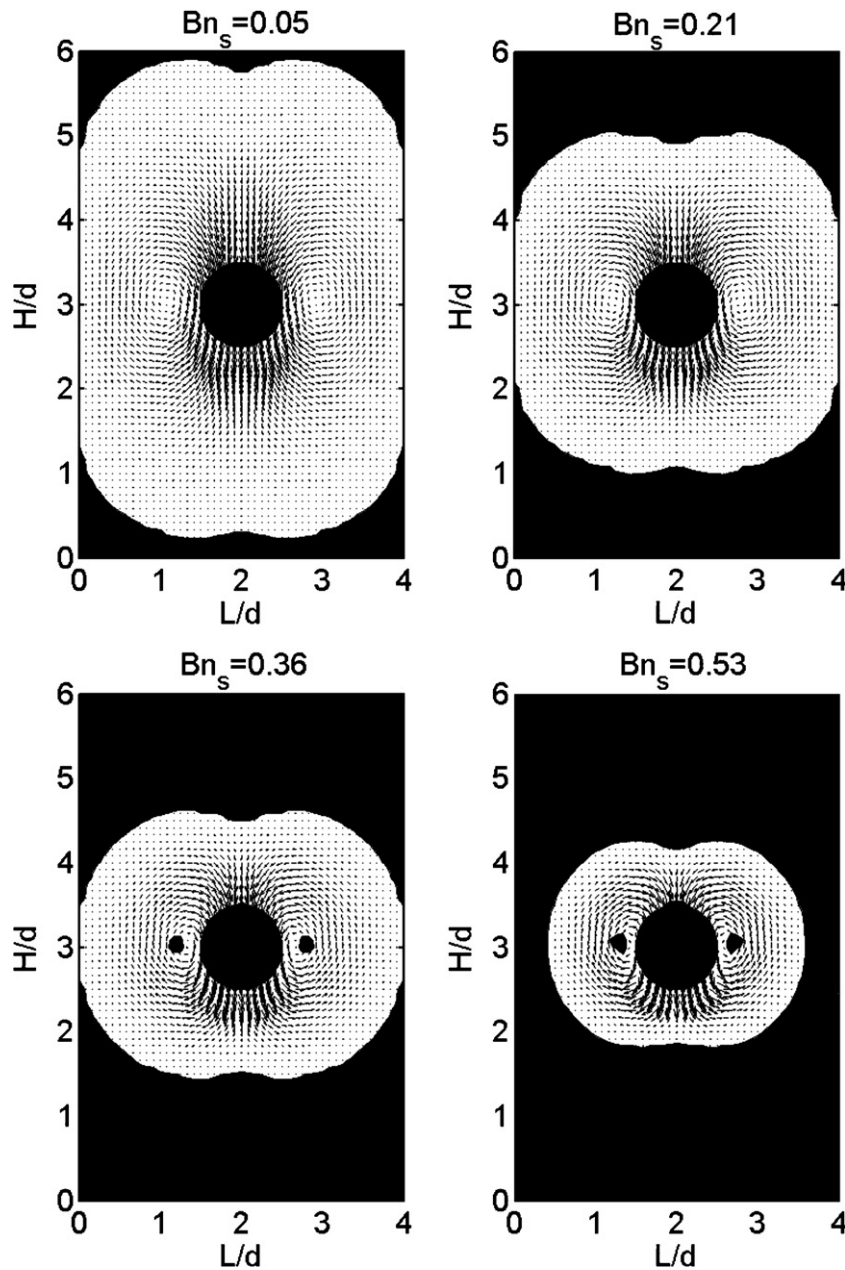
Fig. 14. Yielded (white)/unyielded (black) region together with velocity vectors for a sphere settling in a square cylinder filled with Bingham liquid; $Re_S = 1$.

The simulations are performed with various values of the yield stress of the liquid (Bn_S = 0.05, 0.21, 0.36, 0.53, 0.60, 0.66, 0.72). The settling velocity and distance travelled by a sphere falling in a Bingham liquid with Bn_S = 0.21, 0.53 are plotted in Fig. 13 as a function of time. Clearly, the terminal velocity decreases with increase in the yield stress of the Bingham liquid. The unyielded and yielded regions and steady state velocity vectors are shown in Fig. 14. As already observed with the fixed sphere, the confinement of the sphere by the unyielded region increases progressively with the increase of the yield stress. The shape and extent of these regions are in qualitative agreement with the literature (Beris et al., 1985; Blackery & Mitsoulis, 1997; Liu et al., 2002; Yu & Wachs, 2007). The recirculating regions observed on both sides of the sphere are consequences of the finite size of the square cylinder. It is clear that the centers of recirculating regions shift closer to the sphere with an increase of the Bingham number which is qualitatively similar to the results reported in the literature (Beris et al., 1985; Blackery & Mitsoulis, 1997).

A quantitative comparison of our results with those reported in the literature is shown through the variation of the velocity ratio (U_∞/V) with Bingham number (Bn_S) in Fig. 15. The results show some variability; with our results slightly (but systematically) higher than those from the available literature (that are not conclusive as well) especially at moderate to high Bingham numbers ($Bn_S > 0.36$). The possibility of considerable influence due to the cylinder walls is quite unlikely at such high Bingham numbers ($Bn_S = Bn_T/\nu_r$, and thus $Bn_S = 0.36$ corresponds to $Bn_T = 2.4$) as discussed for the fixed sphere cases.

5. Double sphere sedimentation

In this section, we investigate the hydrodynamic interaction between the two spheres falling along the axis of symmetry of a square cylinder at low and moderate Reynolds number. Hydrodynamic interaction is interpreted in terms of settling velocity, flow
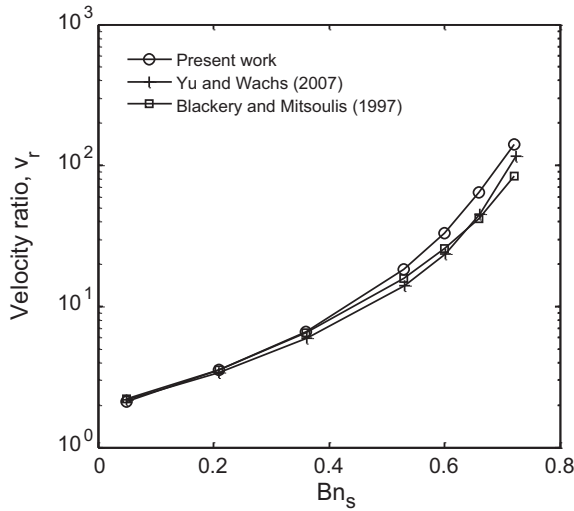
Fig. 15. Velocity ratio (v_r) as a function of Bingham number (Bn_S) when sphere settles under the effect of gravity; $Re_S = 1$; comparison with the literature results (Blackery & Mitsoulis, 1997; Yu & Wachs, 2007).

field and relative velocity of the spheres. The flow definition for sedimentation of two spheres in Bingham liquid is shown in Fig. 16. Zero velocity conditions are applied on all boundaries while the sphere surface follows the no-slip condition.

5.1. Hydrodynamic interaction with low Re

In the first instance inertial effects are considered low, i.e. Re = 1. The Bingham number has a fixed value (Bn = 0.36) and the grid size chosen for the simulations is $4 \times 4 \times 16$ ($L/d \times L/d \times H/d$) with (again) $d = 12$ as the spatial resolution. Initially the spheres are placed along the axis of symmetry with trailing sphere's location $2 \times 2 \times 10$ ($L/d \times L/d \times H/d$). To examine the hydrodynamic interaction, the numerical experiments are performed with a range of center to center distances ($W/d = 1.0, 1.25, 1.5, 2.0, 2.5, 3.0, 3.5$) betwe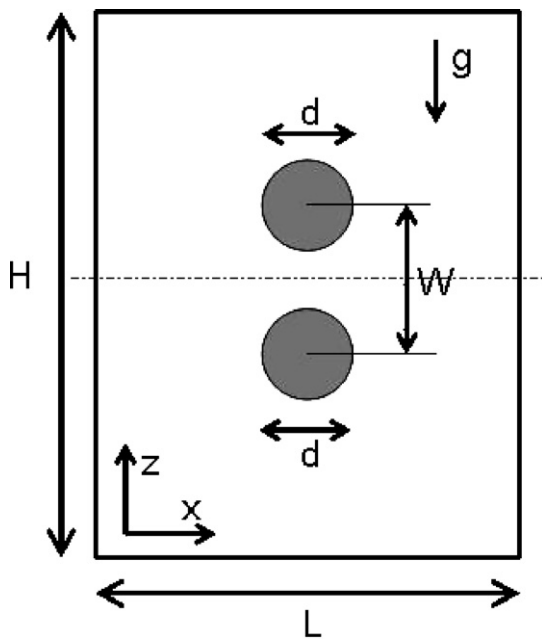en the two spheres. How we evolve to a steady settling velocity is shown in Fig. 17 for some W/d ratios. It is obvious from the figure that both the spheres initially accelerate with equal rate and ultimately move with equal terminal velocity. Therefore it is concluded that both the spheres maintain the initial distance throughout their motion and the trailing sphere does not approach the leading sphere. Fig. 17 also reveals that the terminal velocity of the spheres becomes higher as their separation distance decreases. The terminal velocity of two spheres is always equal or higher than the terminal velocity of a single sphere settling under the same conditions. The leading sphere behaves as a shield to the trailing sphere which experiences a smaller drag force as compared to the leading sphere. Treating the two spheres like a single body, the mass and thus the weight of the whole body is doubled however the drag force on the whole body is much less than twice the drag force experienced by a single sphere. Therefore one obtains a higher terminal velocity of the sphere doublet in comparison to that of a single sphere settling under similar conditions.

A quantitative depiction of the hydrodynamic interaction (in terms of terminal velocity of two spheres) with W/d ratio is shown in Fig. 18 where U_1 and U_2 are the terminal velocities of a single sphere and two spheres, respectively settling in a finite size container filled with Bingham liquid under similar conditions. When the two spheres are at a large distance ($W/d > 3.5$), they hardly interact and the terminal velocity of either sphere is equal to the terminal velocity of single sphere settling under the same conditions. Our results show the same pattern as observed by Yu and Wachs (2007). The deviations appearing in the figure are most likely due to the difference in geometry. Yu and Wachs (2007) used a cylinder with circular cross-section whose diameter is four times the diameter of sphere while we have used a cylinder with square cross-section whose sides are four times the diameter of the sphere. Due to this geometry difference, we observe less pronounced wall effects. The new force balance equation for a single sphere sedimentation in a finite size container is written as

$$F_G = F_D + F_B + F_W \tag{13}$$

where F_G, F_D, F_B and F_W are gravitational force, drag force, buoyancy force and force due to wall effects on a single sphere, respectively. In case of two identical spheres (one above the other) sedimentation, the force balance equation is

$$2F_G = F'_D + 2F_B + F'_W \tag{14}$$

with F'_D and F'_W being the drag force and force due to walls, respectively on the sphere doublet. Combining Eqs. (13) and (14) we obtain:

$$F'_W = 2F_W + 2F_D - F'_D \tag{15}$$

If the two spheres are not very far from each other, the drag force on the sphere doublet F'_D is less than the twice the drag force on a single sphere, i.e. $2F_D - F'_D > 0$. Using this condition one can deduce that $F'_W > 2F_W$. Therefore it is concluded that each sphere of a sphere doublet, settling in a finite size container, experiences a higher retardation effect due to wall in comparison to a single sphere sedimenting alone in same conditions. This implies that the value of U_1/U_2 increases with stronger wall effects. This is supported by the fact that values of U_1/U_2 obtained by our simulations are approximately 7% (on average) lower than those obtained by Yu and Wachs (2007).

In Fig. 19 we display the steady state velocity vectors coupled with yielded and unyielded regions for various W/d ratios. When the two spheres are at distances of 2.5d and 3d, the flow field and yielded envelope around a sphere is similar to those observed with a single sphere. Apart from the islands of unyielded regions appearing on either side of a sphere, there are other unyielded regions in the yielded envelop. They include the regions along the mid plane; along the axis of symmetry between the spheres and on the poles of
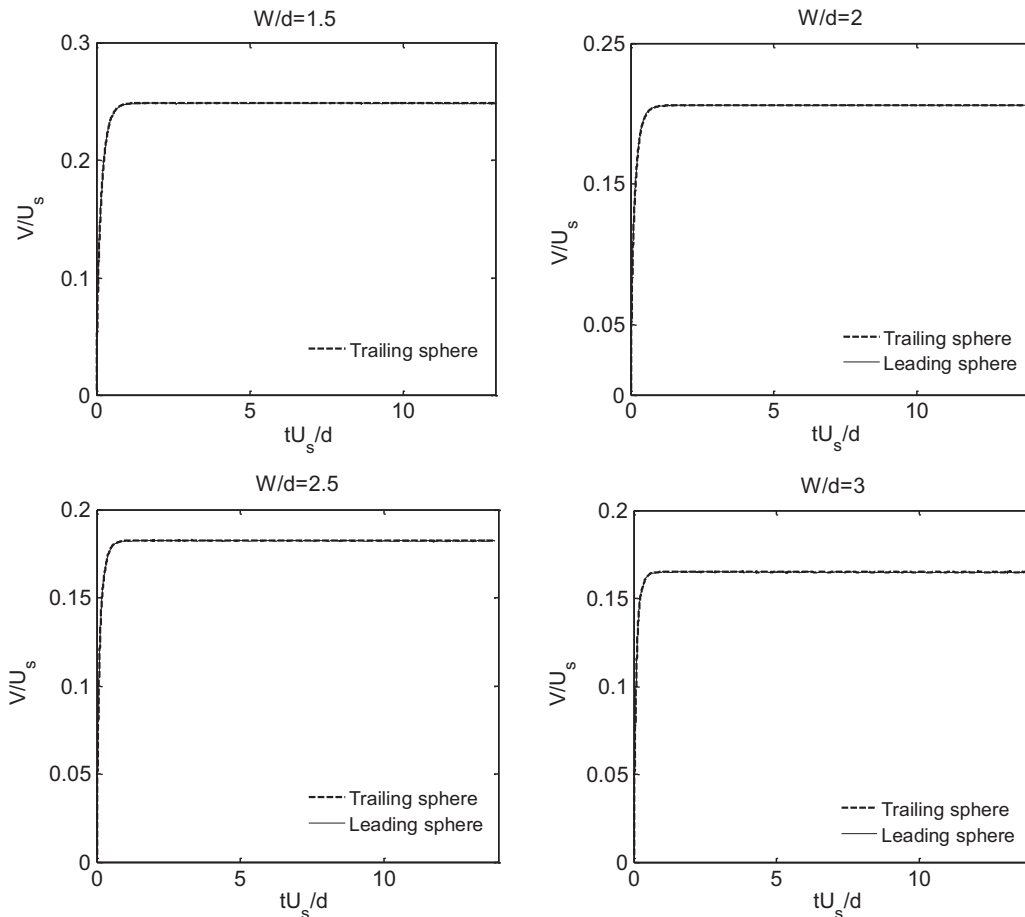

Fig. 16. Flow definition of sedimentation of two spheres in a cylinder of square cross-section ($L \times L$) filled with Bingham liquid.

Fig. 17. Time series of settling velocities of two spheres in Bingham liquid with different W/d ratios; Re = 1 and Bn = 0.36.

the spheres. The unyielded regions along the mid plane and symmetry axis are caused by the re-circulation which is essential for mass conservation within the yielded envelope. We do not observe the polar caps on both sides of the spheres which are expected because of the stagnation points. Liu et al. (2003) and Yu and Wachs (2007) also reported the disappearance of polar caps in their numerical results. The reason, as pointed out by Liu et al. (2003), is that the

Fig. 18. U_1/U_2 as a function of W/d ratio; U_1 is settling velocity of single sphere; U_2 is settling velocity of sphere doublet; comparison with the literature result (Yu & Wachs, 2007).

polar cap regions are too small to be detected in the simulations with the present grid size. Use of a finer grid may shed some insight into the issue. The size of the unyielded regions along the planes decreases with the decrease of separation distance. The unyielded regions situated between the spheres along the axis of symmetry also decrease in size with decreasing separation distance. However, it becomes larger after bringing the spheres still closer (see the W/d = 1.5 panel of Fig. 19). The small islands of unyielded regions at either side of spheres vanish with decreasing separation distance. The flow field and yielded/unyielded regions reported in the present work are in good agreement with the literature (Liu et al., 2003; Yu & Wachs, 2007).
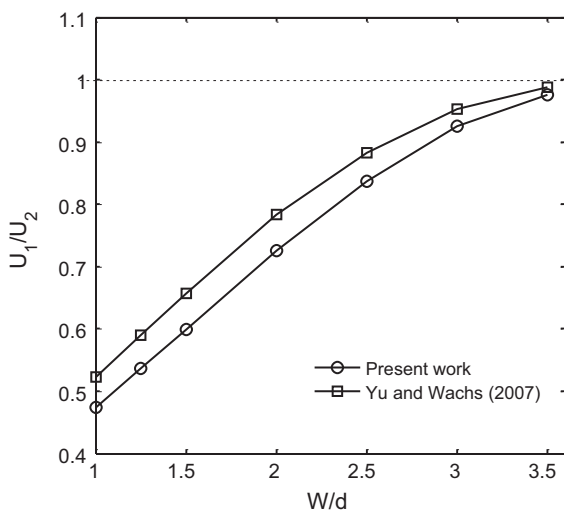
5.2. Hydrodynamic interaction with moderate Re

We do some simulations to see what happens when two spheres fall one above the other in Bingham liquid at moderate Reynolds number. For this case the Reynolds number (Re) is 6.2, Bingham number (Bn) is 0.36 and the grid size used is $4 \times 4 \times 80$ ($L/d \times L/d \times H/d$) with d = 12. The two spheres, placed initially at a center to center distance of $2d$ along the axis of symmetry fall in Bingham liquid under the influence of gravity. The starting position of the trailing sphere is kept as $2 \times 2 \times 58$ ($L/d \times L/d \times H/d$). The time series of settling velocity of the spheres and the distance covered by them are displayed in Fig. 20. It is obvious from the figure that the trailing sphere moves faster than the leading sphere. The velocity vectors and yielded/unyielded regions are drawn at three different times (tU_∞/d = 0.43, 22, 48) and shown in Fig. 21. During the initial stages (e.g. tU_∞/d = 0.43) when the flow is partially devel-
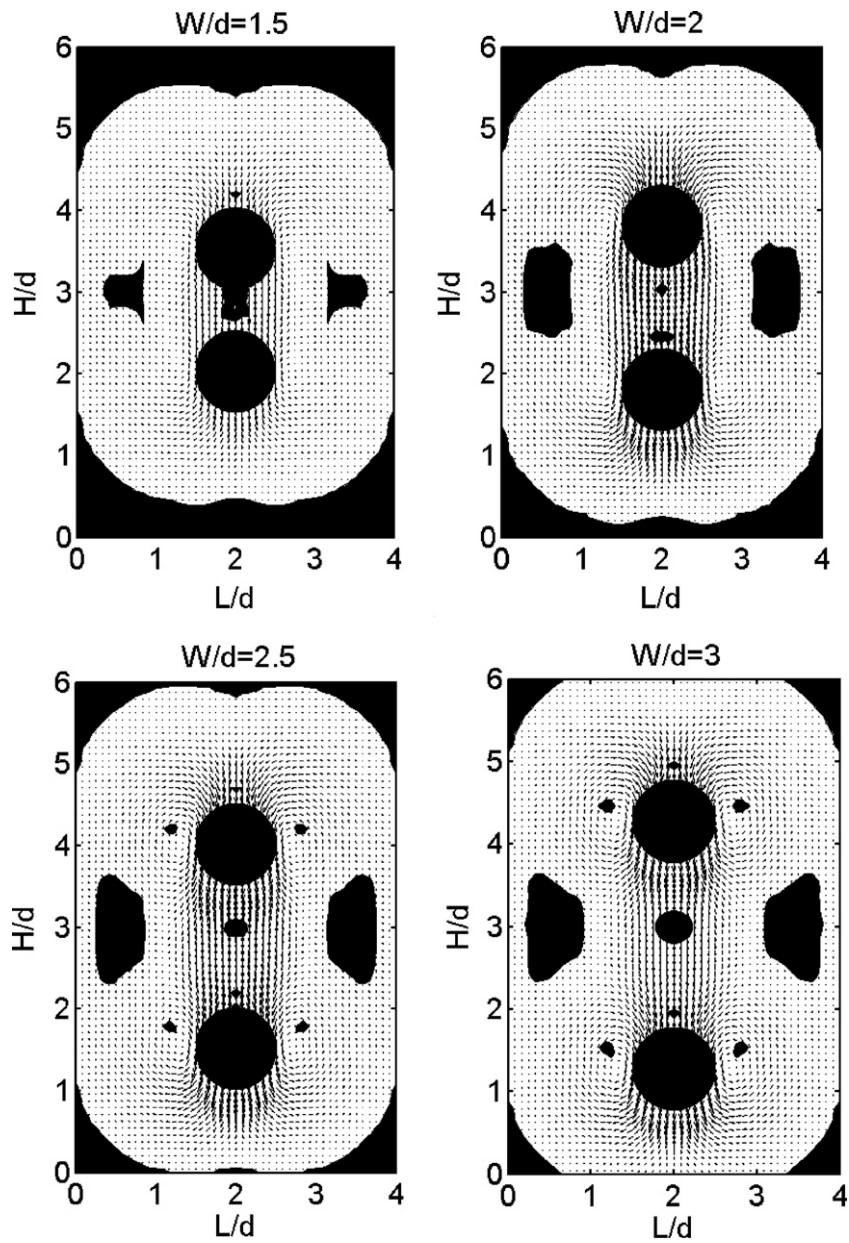
Fig. 19. Steady state velocity vectors coupled with yielded (white)/unyielded (black) regions for settling of the two spheres in a Bingham liquid with different W/d ratios; $Bn = 0.36$ and $Re = 1$.
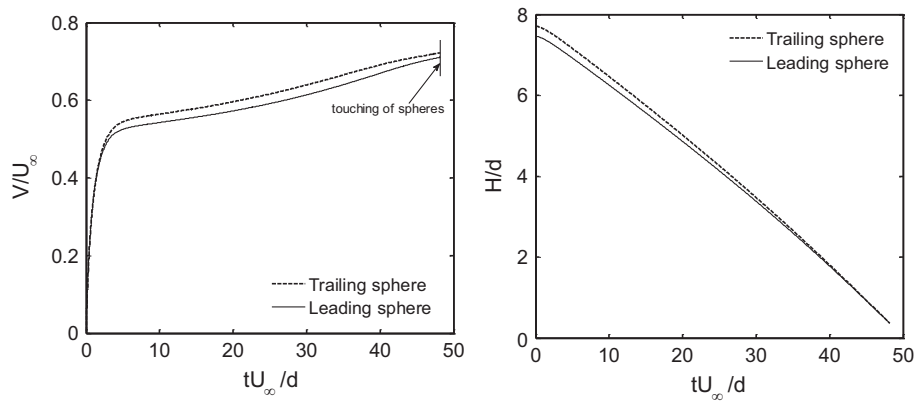

Fig. 20. Time series of (left) settling velocity and (right) traveled distance of the two spheres in a Bingham liquid with initially $W/d = 2$; $Re = 6.2$; $Bn = 0.36$.
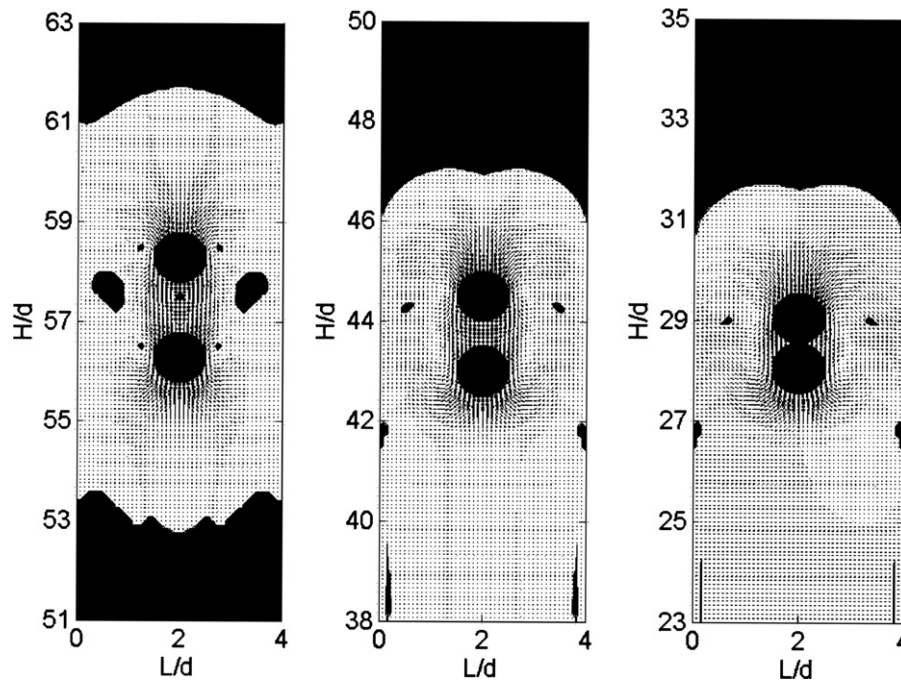
Fig. 21. Velocity vectors coupled with yielded (white)/unyielded (black) regions for settling of the two spheres in a Bingham liquid at time periods (left) $tU_\infty/d = 0.43$ (middle) $tU_\infty/d = 25$ (right) $tU_\infty/d = 48$; Re = 6.2; Bn = 0.36.

oped and the spheres are far from each other, the unyielded regions appear along the mid plane, along the axis of symmetry between the spheres and at either side of each sphere. As the flow develops, the yield effects are softened due to the inertial forces and the unyielded regions along the axis of symmetry and on either side of the sphere vanish. At this moment this system behaves like two spheres sedimenting in a Newtonian liquid where the low pressure region in the vicinity of leading sphere's wake draws the trailing sphere towards itself. In case of low Reynolds number there is an unyielded region along the axis of symmetry between the spheres which prevents the trailing sphere to approach the leading sphere.

6. Concluding remarks

A direct simulation strategy for solving the motion of spherical particles in Bingham liquid has been presented in this paper. First, the implementation of Bingham rheology is validated with lid-driven cavity flow as a benchmark. At low Reynolds number, the vertical position of the primary vortex and the vortex intensity are functions of the Bingham number. In this respect, our results showed good quantitative agreement with those reported in the literature (Mitsoulis & Zisis, 2001; Yu & Wachs, 2007) that were obtained with different numerical methods. The horizontal position of the primary vortex remains insensitive at low Reynolds number. At higher Reynolds number, the yield effects are softened and vertical as well as horizontal positions of primary vortex are appreciably affected (again in agreement with the literature, Vola et al., 2003). While studying the lid-driven cavity flow at different Reynolds numbers, the horizontal position of the primary vortex is found to be more sensitive (as compared to vertical position) with respect to Reynolds number.

Applying the simulation strategy to two phase systems, the interaction of a sphere with Bingham liquid at low Reynolds number is strongly affected by the yield stress of the liquid. The drag force calculated in case of Bingham flow past a fixed sphere increases with increase of yield stress, largely in quantitative agree-

ment with results due to Blackery and Mitsoulis (1997). Deviations could be attributed to differences in the flow geometry (round versus square containers).

Similarly the settling velocity of a single sphere sedimenting in Bingham liquid is a distinct function of liquid's yield stress. It decreases with the increase of yield stress. In case of a single sphere falling in Bingham liquid under the effect of gravity, we observe some quantitative deviations from the literature (viz. Blackery & Mitsoulis, 1997; Yu & Wachs, 2007) at moderate to high Bingham numbers. These deviations could be partly due to the differences in numerical methods and partly due to the differences in the shape of the flow domain (rectangular versus circular cross-section).

A low Reynolds number study of sedimentation of two spheres in Bingham liquid suggests the increased hydrodynamic interaction with decrease in separation distance between the spheres. There exists an unyielded region between the two spheres due to which the spheres do not approach each other. The spheres move with equal settling velocity which is always equal or greater than the settling velocity of single sphere sedimenting under the same conditions. We observe some quantitative deviations with the literature (Yu & Wachs, 2007). However these deviations are due to the different geometries and are explained by considering wall effects. With increase of inertial forces (moderate Re), the unyielded region between the two spheres vanishes. Due to the interaction with wake of the leading sphere, the trailing sphere approaches the leading sphere, just as it does in the Newtonian case (Fortes, Joseph, & Lundgren, 1987).

In future it would be interesting to implement a collision model which allows for a proper resolution of particle–particle interaction – in line with the recent paper by Wachs (2009) – and then examine the tumbling behavior of the two spheres and check whether they aggregate or not. The hydrodynamic interaction between more than two particles is a desirable condition to asses the role of multiparticle interactions on the settling velocity. Therefore it is required to carry out the simulations with more than two particles with different orientations. Further as a generalization of the numerical tool, various particle shapes can be considered and the impact of their hydrodynamic interactions on the setting velocity can be

determined so that (eventually) we will be able to directly simulate the dynamics of dense suspensions involving Bingham liquids.

References

Abraham, F. (1970). Functional dependence of drag coefficient of a sphere on Reynolds number. *Physics of Fluids*, *13*, 2194.

Ansley, R. W., & Smith, T. N. (1967). Motion of spherical particles in a Bingham plastic. *AICHE Journal*, *13*, 1193.

Beris, A. N., Tsamopoulos, J. A., Armstrong, R. C., & Brown, R. A. (1985). Creeping motion of a sphere through a Bingham plastic. *Journal of Fluid Mechanics*, *158*, 219.

Beverly, C. R., & Tanner, R. I. (1992). Numerical analysis of three-dimensional Bingham plastic flow. *Journal of Non-Newtonian Fluid Mechanics*, *42*, 85.

Blackery, J., & Mitsoulis, E. (1997). Creeping motion of a sphere in tubes filled with a Bingham plastic material. *Journal of Non-Newtonian Fluid Mechanics*, *70*, 59.

Botella, O., & Peyret, R. (1998). Benchmark spectral results on the lid-driven cavity flow. *Computers & Fluids*, *27*(4), 421.

Chen, S., & Doolen, G. D. (1998). Lattice Boltzmann method for fluid flows. *Annual Review of Fluid Mechanics*, *30*, 329.

Derksen, J. J. (2008). Flow-induced forces in sphere doublets. *Journal of Fluid Mechanics*, *608*, 337.

Derksen, J. J., & Sundaresan, S. (2007). Direct numerical simulations of dense suspensions: Wave instabilities in liquid-fluidized beds. *Journal of Fluid Mechanics*, *587*, 303.

Derksen, J., & Van den Akker, H. E. A. (1999). Large eddy simulations on the flow driven by a rushton turbine. *AIChE Journal*, *45*, 209.

Eggels, J. G. M., & Somers, J. A. (1995). Numerical simulation of free convective flow using the lattice-Boltzmann scheme. *International Journal of Heat and Fluid Flow*, *16*, 357.

Fortes, A., Joseph, D. D., & Lundgren, T. (1987). Nonlinear mechanics of fluidization of beds of spherical particles. *Journal of Fluid Mechanics*, *177*, 467.

Gartling, D. K., & Phan-Thien, N. (1984). Numerical simulation of a plastic fluid in a parallel-plate plastometer. *Journal of Non-Newtonian Fluid Mechanics*, *14*, 347.

Iwaoka, M., & Ishii, T. (1979). Experimental wall correction factors of single solid spheres in circular cylinders. *Journal of Chemical and Engineering Japan*, *12*, 3.

Liu, B. T., Muller, S. J., & Denn, M. M. (2002). Convergence of a regularization method for creeping flow of a Bingham material about a rigid sphere. *Journal of Non-Newtonian Fluid Mechanics*, *102*, 179.

Liu, B. T., Muller, S. J., & Denn, M. M. (2003). Interactions of two rigid spheres translating collinearly in creeping flow in a Bingham material. *Journal of Non-Newtonian Fluid Mechanics*, *113*, 49.

Masliyah, J., Zhou, Z. J., Xu, Z., Czarnecki, J., & Hamza, H. (2004). Understanding water-based bitumen extraction from Athabasca oil sands. *Canadian Journal of Chemical Engineering*, *82*, 628.

Merkak, O., Jossic, L., & Magnin, A. (2006). Spheres and interactions between spheres moving at very low velocities in a yield stress fluid. *Journal of Non-Newtonian Fluid Mechanics*, *133*, 99.

Mitsoulis, E., & Zisis, Th. (2001). Flow of Bingham plastics in a lid-driven square cavity. *Journal of Non-Newtonian Fluid Mechanics*, *101*, 173.

Miyamura, A., Iwasaki, S., & Ishii, T. (1981). Experimental wall correction factors of single solid spheres in triangular and square cylinders, and parallel plates. *International Journal of Multiphase Flow*, *7*, 41.

O'Donovan, E. J., & Tanner, R. I. (1984). Numerical study of the Bingham squeeze film problem. *Journal of Non-Newtonian Fluid Mechanics*, *15*, 75.

Papanastasiou, T. C. (1987). Flow of materials with yield. *Journal of Rheology*, *31*, 385.

Peysson, Y. (2004). Solid/liquid dispersions in drilling and production. *Oil Gas Science and Technology Reviews IFP*, *59*, 11.

ten Cate, A., Nieuwstad, C. H., Derksen, J. J., & Van den Akker, H. E. A. (2002). Particle imaging velocimetry experiments and lattice-Boltzmann simulations on a single sphere settling under gravity. *Physics of Fluids*, *14*, 4012.

Vola, D., Boscardin, L., & Latche, J. C. (2003). Laminar unsteady flows of Bingham fluids: A numerical strategy and some benchmark results. *Journal of Computational Physics*, *187*, 441.

Wachs, A. (2009). A DEM-DLM/FD method for direct numerical simulation of particulate flows: Sedimentation of polygonal isometric particles in a Newtonian fluid with collisions. *Computers & Fluids*, *38*, 1608.

Yu, Z., & Wachs, A. (2007). A fictitious domain method for dynamic simulation of particle sedimentation in Bingham fluids. *Journal of Non-Newtonian Fluid Mechanics*, *145*, 78.